From asynchronous states to Griffiths phases and back: Structural heterogeneity and homeostasis in excitatory-inhibitory networks

Jorge Pretel,[1] Victor Buendía,[2,3] Joaquín J. Torres,[1] and Miguel A. Muñoz[1]

[1]*Departamento de Electromagnetismo y Física de la Materia and Instituto Carlos I de Física Teórica y Computacional, Universidad de Granada, 18071 Granada, Spain*

[2]*Deparment of Computer Science, University of Tübingen, Tübingen, Germany*

[3]*Max Planck Institute for Biological Cybernetics, Tübingen, Germany*

(Received 6 October 2023; accepted 26 February 2024; published 4 April 2024)

Balanced neural networks, in which excitatory and inhibitory inputs compensate each other on average, give rise to a dynamical phase dominated by fluctuations called an asynchronous state, crucial for brain functioning. However, structural disorder, which is inherent to random networks, can hinder such an excitation-inhibition balance. Indeed, structural and synaptic heterogeneities can generate extended regions in phase space akin to critical points, called Griffiths phases, with dynamical features very different from those of asynchronous states. Here we study a simple neural-network model with tunable levels of heterogeneity able to display these two types of dynamical regimes, i.e., asynchronous states and Griffiths phases, putting them together within a single phase diagram. Using this simple model, we are able to emphasize the crucial role played by synaptic plasticity and homeostasis to reestablish balance in intrinsically heterogeneous networks. Overall, we shed light onto how diverse dynamical regimes, each with different functional advantages, can emerge from a given network as a result of self-organizing homeostatic mechanisms.

DOI: 10.1103/PhysRevResearch.6.023018

I. INTRODUCTION

Understanding the relationship between the basic structural features of a neural network and its dynamical repertoire is crucial if one aims to construct a general modeling framework to describe brain function [1–3]. Neural populations must be able to effectively process incoming signals while keeping their activity sparse and segregated from other areas involved in different tasks and might need to transmit their outputs to other regions to integrate information at a higher level [4,5]. This segregation-integration balance is severely constrained by the spatial distribution and connectivity patterns of different cells [6,7].

Recent advances in recording techniques allow for the measurement of the activity of thousands of neighboring cortical neurons in a rather accurate manner, revealing that cells tend to fire in an irregular fashion with high variability and relatively low average pairwise correlation [8–11]. This type of empirically observed collective dynamical regime, known as an asynchronous state [12–15], is theoretically understood as the outcome of the interplay between the opposing excitatory and inhibitory forces that together control the dynamical state of neural populations [9,15–21]. More specifically, when the connectivity pattern is such that excitatory and inhibitory inputs to any given neuron nearly compensate each other on average, the activity of such a cell is dominated by fluctuations of the input rather than by its mean value, which may be below threshold. As a consequence, the resulting asynchronous state of balanced networks is characterized by sporadic firing events with high temporal variability, akin to a random Poisson process [16–20].

Early theoretical and modeling approaches succeeded at reproducing this fluctuation-dominated asynchronous state considering sparse random networks and/or synaptic weights that were scaled down with network size [16–18,22]. In particular, sparsity ensures that two given neurons share a negligible proportion of presynaptic neighbors and inputs, and hence their activity remains mostly uncorrelated. However, actual cortical populations are known to be densely connected [23,24]. Thus, the prerequisite of network sparsity was later relaxed and more-refined models introduced the possibility of a dynamical balance, by which the temporal variations in excitatory input could be rapidly tracked and compensated by variations of the inhibitory counterpart, leading to low pairwise correlations even in densely connected networks [15]. In particular, although pairwise correlations are consistently found to be small on average in empirical measurements of neural activity, more recent studies have reported nontrivial correlation structures in cortical circuits, such as nonmonotonic dependences on distance [25], heterogeneous synaptic connections [26–28], and correlation patterns extending across ranges considerably larger than the typical reach of local synaptic connections [29,30]. These correlations give rise to so-called neural modes, i.e., specific activation patterns that capture the bulk of activity variability in cortical populations, which are robustly observed and have been proven to be crucial for brain

functioning [10,31–33]. Improved models account also for these features and thus the asynchronous-state paradigm of neural dynamics has become something of the standard model in computational neuroscience [15,19,25,26,29,34].

In parallel to these findings, recorded neuronal activity, in both local circuits [35–37] and whole-brain measurements [38–40], reveals the widespread occurrence of neuronal avalanches, i.e., highly heterogeneous cascades of spontaneous activity characterized by scale invariance in space and time [41–48]. Power-law scaling in avalanche size and duration distributions constitutes a hallmark of critical behavior in stochastic models of propagating activity such as the branching process (see, e.g., [49]). Scale-free avalanching behavior appears when the system is placed at a critical point, i.e., at the edge of a transition separating a quiescent phase, where activity decays to zero, and an active one, where activity is self-sustained. The critical state is characterized by the divergence of physical quantities such as the correlation length and response to perturbations and has been argued to entail important functional advantages for biological systems [41–45,50–52]. In particular, it has been shown that neural-network functional properties such as dynamic range, information transmission, and information capacity can be optimized by setting the network dynamical state close to the edge of a phase transition [43,44,50,53–57].

Let us highlight that the mostly uncorrelated activity of asynchronous states stands in contrast to the huge spatiotemporal correlations near critical states [58–60]. To understand this seeming dichotomy between asynchronous and critical states, a crucial aspect of neural networks such as network heterogeneity needs to be considered further. Indeed, an essential feature of actual neuronal networks is that they are far from regular; thousands of interconnected cells cluster together in the cortex, forming a diverse and irregular set of motifs [24,50,61,62]. Such an inherent heterogeneity entails the emergence of local variability in neuronal densities, neuronal types, and coupling strengths, giving rise to a complex structural architecture, which in turn is at the basis of an emergent rich dynamical behavior [26,63–67]. The resulting complex structural and dynamical patterns constitute a substrate for the emergence of varied and intricate computational processes at the bases of cognitive functions, a richness that does not emerge in perfectly regular substrates. Structural disorder consequently plays a primary role in defining the emergent collective behavior and therefore the functional capabilities of a neural network.

From the theory of critical phenomena [44,68,69] we know that the introduction of structural heterogeneity or disorder, in the form of, for example, diverse coupling strengths among neurons or in their spacial localization, may induce the emergence of rare-region effects, namely, the spontaneous formation of atypical local clusters with behavior differing from the network average. Such clusters exert an influence on nearby units, leading to nontrivial collective dynamical properties of disordered systems [70–72]. In particular, it has been reported that heterogeneous networks embedded in a physical space can display an extended region in parameter space, called a Griffiths phase, with critical-like features such as generic power laws in avalanche distributions with varying exponents, slow dynamics, divergence in response to stimuli, etc. [73–77]. This stretching of a critical point into a broad region, besides relaxing the need for fine-tuning that characterizes criticality in ordered systems, is likely to emerge in systems such as brain networks embedded in a physical space and with a highly heterogeneous connectivity pattern [75]. On the other hand, high degrees of heterogeneity can severely hinder the possibility of achieving a local excitatory-inhibitory balance, so it seems that the asynchronous state itself might be compromised by the presence of heterogeneity. In particular, heterogeneity in the spatial location of excitatory and inhibitory neurons could possibly lead to a situation where recurrent activity is concentrated in excitation-dominated regions while the rest of the network might be inhibition dominated and thus remain mostly silent [78].

Our aim here is to investigate a very simple network model of binary neurons such that it supports the two main paradigms of dynamical behavior in cortical networks: (i) an asynchronous phase and (ii) an extended critical-like region, i.e., a Griffiths phase. Employing networks with a tunable degree of heterogeneity, we scrutinize the effects of spatial structural disorder on the emergence and possible coexistence of these two diverse dynamical regimes. In particular, we show that for a regular network embedded in a physical (Euclidean) space there is an asynchronous state with roughly equal excitatory and inhibitory inputs to each single neuron. However, this balance breaks down as the degree of heterogeneity is increased by randomly redistributing a fraction of neurons in space. Thus, spatial heterogeneity generates a state in which the activity reverberates for extended periods in local overexcited clusters while inhibition-dominated areas produce local quiescent states, i.e., a Griffiths phase. Furthermore, we study the effect of two different homeostatic mechanisms regulating the local dynamics through the modification of synaptic weights, showing that both of them are able to dynamically restore the structurally broken excitatory-inhibitory balance and generate self-organized balanced networks with a standard critical point rather than a Griffiths phase, in spite of the heterogeneous spatial distribution of neurons.

II. MODEL AND METHODS

We consider a simple rate model of binary neurons (introduced in previous works [20,79] and similar to [80]) that aims to capture the key ingredients of neural-network collective dynamics in a parsimonious way. The model consists of a network with N neurons, a fraction $\alpha = 0.8$ of which are excitatory (E) while the rest are inhibitory (I). Each neuron $i \in [1, 2, \ldots, N]$ can be in either an active state $s_i(t) = 1$ or a quiescent state $s_i(t) = 0$ and it projects to every other neuron within a circle of a given radius σ_k, with $k = E, I$ (see below and Fig. 1 for a model sketch of the network architecture).

At every discrete time step $t = 1, 2, \ldots$, each neuron i integrates all the weighted inputs from its neighboring (presynaptic) neurons

$$\Lambda_i = \frac{\gamma}{k_i} \sum_j \omega_{ij} s_j(t), \tag{1}$$

where ω_{ij} are the corresponding synaptic weights from neuron j to neuron i (positive for excitatory j neurons $\omega_E > 0$ and negative for inhibitory ones $\omega_I < 0$), k_i is the in-degree

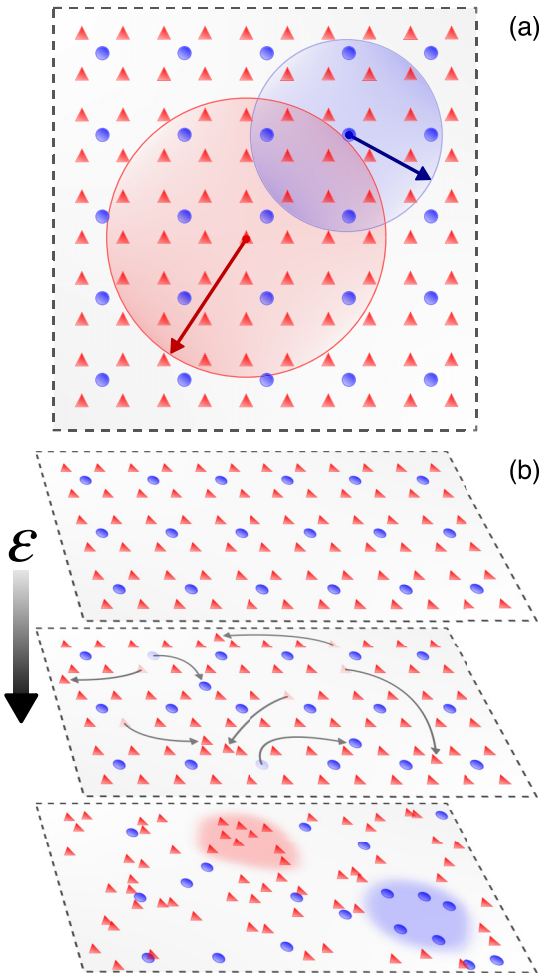

FIG. 1. Network topology: from homogeneous to heterogeneous network architectures. (a) Spatial connectivity pattern defining a regular network (lattice) embedded in a two-dimensional substrate ($\varepsilon = 0$). Note that 80% of the neurons are excitatory (red) and the remaining 20% are of inhibitory (blue). Each excitatory (E) or inhibitory (I) neuron projects synapses or connections to all other neurons within a given radius $\sigma_{E,I}$ (red and blue circles for excitatory and inhibitory neurons, respectively). (b) Starting from the regular lattice, a fraction ε of all neurons is randomly relocated, thus generating regions (such as the red shaded one) where excitatory neurons are overrepresented as well as inhibition-dominated zones (such as the blue shaded one). As ε increases, more heterogeneous networks can be constructed (see the vertical arrow). The presence of large rare regions with unbalanced connectivity patterns (marked with red and blue shaded areas in the lowest panel) influences dramatically the dynamical regime on such heterogeneous networks.

of the ith neuron (used to normalize as in previous works [77,81,82]), and γ represents an overall coupling strength that modulates the influence of neighboring neurons and serves as an overall control parameter. If neuron i is quiescent ($s_i = 0$), it becomes active with a probability $\mathcal{P}_i = f(\Lambda_i)$, where f is a nonlinear (piecewise linear) transfer function

$$f(\Lambda_i) = \begin{cases} 0, & \Lambda_i < 0 \\ \Lambda_i, & 0 \leqslant \Lambda_i \leqslant 1 \\ 1, & \Lambda_i > 1. \end{cases}$$

Conversely, if the focal neuron is active $s_i = 1$, then it becomes quiescent with complementary probability $1 - \mathcal{P}_i$.

The choice of $f(x)$ as a piecewise linear function is made for the sake of simplicity; however, even if the kind of nonlinearity can have an impact on some features of the system (as we discussed in Ref. [20]), we have verified that the forthcoming results are robust to the introduction of nonlinearities in the gain function (see Appendix A). Similarly, without loss of generality, the parameter values are fixed to $\omega_E = 1$, $\omega_I = -2.5$, $\sigma_E = 3.4$, and $\sigma_I = 2.3$ (where $\sigma = 1$ is the distance between two nearby E neurons in the regular network).

The previous dynamics is first run on a regular directed network consisting of N neurons embedded in a Euclidean space which, for the sake of simplicity and without loss of generality, we consider to be two dimensional, with periodic boundary conditions. The regular grid has excitatory neurons at positions (i, j), with a single inhibitory neuron per every four excitatory ones (as shown in Fig. 1). Hence, a system of size L has $N = 5L^2/4$ neurons. For most of the analyses, we consider $L = 120$ and $N = 18\,000$.

This homogeneous connectivity pattern enforces that every single neuron has the same number of incoming E and I links (see Fig. 1, top). In order to study the effects of heterogeneity we also analyze the model dynamics on perturbed networks in which the spatial location of each neuron is allowed, with some probability ε, to shift to a new randomly selected position. Thus, $\varepsilon = 0$ describes a perfectly regular network and $\varepsilon = 1$ characterizes a random spatial network (Fig. 1), so the relocation parameter ε allows one to sample different system architectures with tunable levels of heterogeneity.

For the sake of completeness, the spectra of the connectivity matrices for diverse degrees of heterogeneity are shown in Appendix C.

III. RESULTS

The described neuron model has been previously studied on nonspatial regular networks [20,83]. In particular, it has been shown that the presence of a set of inhibitory neurons on sparse networks gives rise to the emergence of an intermediate phase between the standard quiescent phase in which all activity eventually ceases and a phase of saturated activity in which all neurons are active, which does not exist in similar networks composed of only excitatory neurons. This intermediate phase stems from the balance between excitation and inhibition, is dominated by fluctuations, and exhibits all the key statistical properties of asynchronous states (see [15,20]). Thus, from now on we will refer to it as the asynchronous state or phase.

A. Homogeneous case

To go beyond previous results in the literature, we first verified that the same type of phase diagram arises for spatial networks when excitatory and inhibitory neurons are regularly placed in a lattice such as the one in Fig. 1, i.e., for $\varepsilon = 0$. As reported in Fig. 2(a), there is a wide range of coupling values γ that leads to intermediate levels of self-sustained and irregular activity [see Fig. 2(a), top panel; light blue curve]. Such an intermediate phase is separated from a quiescent one, where all activity eventually ceases, by a critical point $\gamma_{c1} \sim 1.365$, as evinced by a marked increase in the variance of the

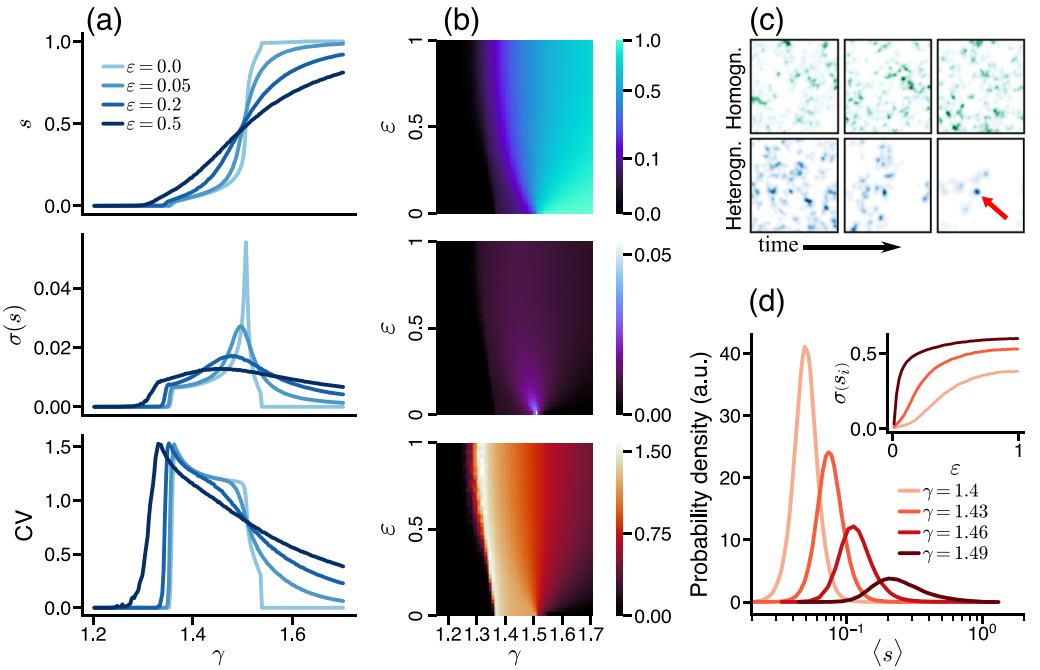

FIG. 2. Phase diagram and main dynamical features. The statistics of the activity for regular and heterogeneous networks are shown. (a) Average activity s (top), activity fluctuations (standard deviation of s, middle), and average coefficient of variation (bottom) for different ε values measured for 100 network realizations along 10^5 time steps (see also Appendix D for a finite-size scaling of the variance). (b) Average activity s (top), activity fluctuations (middle), and CV (bottom) as a function of coupling γ and disorder ε. (c) Slow decay of activity in the Griffiths phase [blue bottom row, $(\gamma, \varepsilon) = (1.30, 0.5)$], displaying an active cluster that exerts influence on its neighboring zone (red arrow), and self-sustained activity in the asynchronous phase for a regular network [green top row, $(\gamma, \varepsilon) = (1.42, 0.0)$]. (d) Distributions of average single-cell activities can show large dispersion even for low heterogeneity levels (data for $\varepsilon = 0.05$ and increasing values of γ). The inset shows the width of the distribution of average single cell activities $\sigma(s_i)$ for increasing ε, for $\gamma = 1.37$, 1.43, and 1.49, from bottom to top; the width of the distributions is zero at $\varepsilon = 0$ and increases more sharply with ε for larger synaptic weights.

overall activity [Fig. 2(a), middle panel]. On the other hand, the asynchronous and the saturated phases are separated by another critical point ($\gamma_{c2} \approx 1.505$), characterized by a more prominent peak in the activity variance [Figs. 2(a) and 2(b), middle panels]. Above this point, inhibition can no longer counteract excitation and the network consequently saturates. Time series illustrating the dynamics for different couplings can be found in Appendix B.

The intermediate phase displays all the essential features of the asynchronous state including irregularity in the spike statistics, as quantified by the coefficient of variation (CV), defined as the quotient between the standard deviation of single-cell interspike intervals (ISIs) and its mean, equal to $\sigma_{\rm ISI}/\mu_{\rm ISI}$.[1] Indeed, as shown in Fig. 2(a) (bottom light blue curve), the CV displays a plateau of highly variable (super-Poissonian) behavior (approximately equal to $1.2 > 1$), which extends to the entire intermediate phase [see Figs. 2(a) and 2(b), bottom panels].

B. Heterogeneous case

When heterogeneous networks are considered, i.e., for $\varepsilon > 0$, the situation becomes qualitatively different, as we describe in what follows. As previously summarized, the density of E and I neurons changes locally in space and this leads to the emergence of a heterogeneous architecture where some local regions become more prone to generate activity due to a locally increased E/I ratio, while in others, activity rapidly decays given the local overabundance of inhibitory neurons (see Fig. 1, bottom panel). This is illustrated in Fig. 2(c), where we plot snapshots of the instantaneous state of activity in the network both for homogeneous (upper panels) and heterogeneous (lower panels) networks, for three different times (starting with an initially saturated state). In the first case activity diffuses across the network in a rather variable way without remaining confined to any spacial location, while in the heterogeneous case it may remain strongly localized in some specific regions (see red arrow), around which it may reverberate for extended durations.

Heterogeneity has also an effect on the single-neuron averaged-activity distributions: These become progressively wider and start developing heavy tails as ε is increased [see the inset of Fig. 2(d), where the variance of such a distribution is plotted as a function of ε for different values of γ].

On the other hand, the steady-state network-averaged activity shifts in a much less abrupt way from the quiescent to saturated phase [Fig. 2(a), top panel] as ε grows. This is due to the gradual recruiting of more and more activity-prone regions as γ is increased [see also Fig. 2(d)]. Similarly, as

[1]The ISI is measured here as the number of time steps between deactivation and consecutive activation of a given cell.

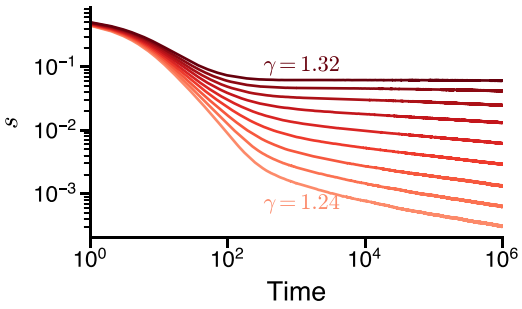

FIG. 3. Griffiths phases in heterogeneous networks. Generic power-law time decay of the network-averaged activity is plotted for diverse values of $\gamma = 1.24, 1.25, \ldots, 1.32$ (from bottom to top) and $\varepsilon = 1.0$. The curves display a continuously varying exponent $s \sim t^{-\alpha(\gamma)}$ for an extended region in γ space, thus defining a Griffiths phase.

heterogeneity increases the peaks in the variance are smoothed out [Fig. 2(a), middle panel], and the CV continues to be larger than 1 in a broad region of γ values [see Fig. 2(a), bottom panel], being increased also for large γ values. Thus, summing up, heterogeneity has the effect of widening the intermediate phase of moderate and fluctuating activity.

The three panels of Fig. 2(b) generalize the previous results for the activity, its variance, and the CV, respectively, by plotting them as a function of both γ and ϵ. Overall, these plots demonstrate that heterogeneity expands the intermediate phase, resulting in a more gradual transition between quiescence and saturation.

We are now set to look for the possible existence of a Griffiths phase for the heterogeneous-network case ($\varepsilon > 0$). As illustrated in Fig. 3, the overall activity (starting from a fully active initial condition) decays as a power law of time all across an extended region in γ space, with continuously changing exponents, which is one of the crucial identifying characteristics of Griffiths phases [73–75]. As usual, the combination of (exponentially) rare large clusters in which activity can reverberate for (exponentially) large times gives rise to this type of scale-free power-law behavior [70,73–75].

Finally, we have verified that heterogeneity yields also changes in the network's response to external inputs. For this, we measured the dynamic range Δ, defined as [84]

$$\Delta = 10 \log \left(\frac{r_{0.9}}{r_{0.1}} \right), \tag{2}$$

where $r_{0.1}$ and $r_{0.9}$ represent the external input intensities r where the system displays 10% and 90% of the maximum possible overall activity, respectively (see the inset in Fig. 4 for an illustration). The external stimulus to each neuron i consists in an additional driving rate r which, in the absence of recurrent input, causes the ith neuron to activate spontaneously with a probability $f(r/k_i)$. As shown in Fig. 4, higher ε values lead to an overall increase in the dynamical range of the network. The peaks around $\gamma \approx 1.35$ and 1.55 in the homogeneous case, coinciding with the transition points, are hallmarks of criticality [84]. Instead, in the heterogeneous case there is a much broader peak with larger values of Δ almost all across the parameter space, which is an identifying characteristic of a Griffiths phase.

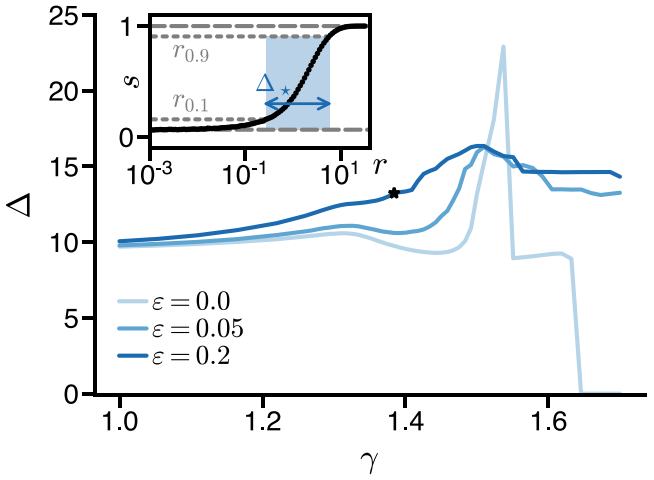

FIG. 4. Griffiths phases in heterogeneous networks. The dynamic range Δ (see the text for details) is plotted as a function of the coupling strength for different heterogeneity levels. The inset shows the mean activity as a function of the external input r for the highlighted point in the main figure; the inset sketches how to compute the dynamic range.

In summary, the asynchronous phase observed in the homogeneous case becomes a Griffiths phase with the introduction of structural heterogeneity.

C. Regulatory mechanisms restore balance

A situation in which a small subset of neurons presents exceptionally high levels of activity while most of the network remains mostly dormant does not seem to be biologically realistic. As a matter of fact, neural networks in the brain employ various strategies to maintain local balance and prevent excessive local activations. Homeostatic mechanisms, such as threshold adaptation, synaptic scaling [85,86], rapid disinhibition, adaptation, and changes in intrinsic excitability, are known to control neuronal firing rates within functionally desirable limits [87–89]. For instance, it has been empirically confirmed that certain types of inhibitory neurons enhance their synaptic strength to neighboring (postsynaptic) neurons if these present exceedingly high firing rates [90]. Thus, following Landau *et al.* [78], we implement a simplified version of the synaptic scaling homeostatic mechanism [85,86,89] in our model for heterogeneous networks.

More specifically, the plasticity mechanism is implemented as follows. Each active inhibitory neuron is assumed to increase the strength of its postsynaptic connections by a certain amount η_p (potentiation), while the synapses of inactive inhibitory neurons are decreased by an amount η_d (depression). In more mathematical terms, the synaptic scaling rule for the synaptic strength of inhibitory neuron i is

$$|\gamma_i(t+1)| = |\gamma_i(t)| + s_i(t)\eta_p - [1 - s_i(t)]\eta_d. \tag{3}$$

Note that this scaling rule uses only local information and that to implement it, the overall synaptic weight γ in Eq. (2) is promoted in Eq. (3) to a neuron-dependent and time-dependent synaptic strength $\gamma_i(t)$ for inhibitory neurons. On the other hand, excitatory weights are kept fixed across the network

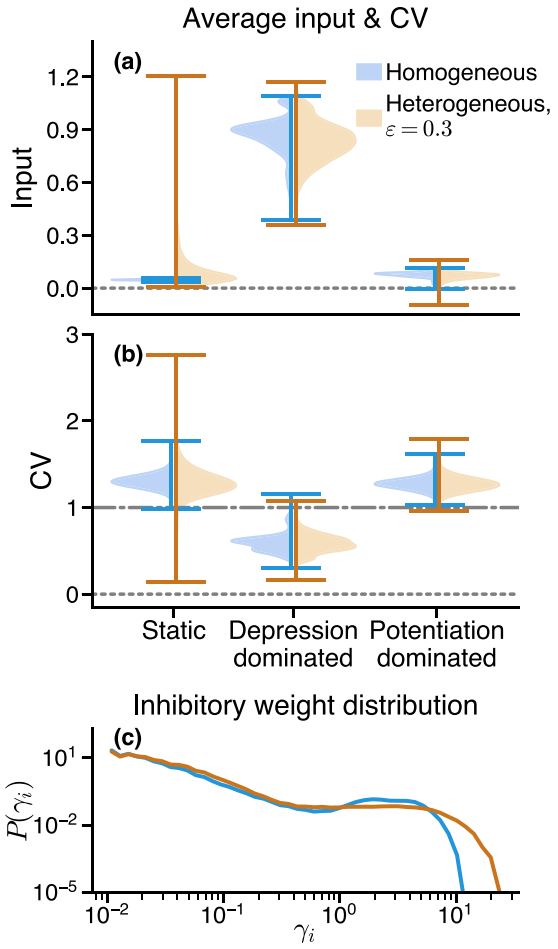

FIG. 5. Effects of homeostatic plasticity. (a) Average input to individual neurons for both homogeneous and heterogeneous networks for static (nonplastic) networks and for two choices of the ratio of $\eta_p = 0.01$ and $\eta_d = 0.1$ (depression dominated) and $\eta_p = 0.1$ and $\eta_d = 0.01$ (potentiation dominated). (b) Distribution of the CV of the ISI of individual neurons for the same cases. Measurements were taken over 10^5 time steps, averaged over 10 realizations, after 10^5 steps. (c) Distribution of weights after 10^6 steps in the potentiation-dominated case. Observe that the distribution is fat tailed. All simulations were performed with $\gamma = 1.4$.

and time. Let us remark that the two plasticity parameters η_p and η_d can be interpreted as the speeds of the underlying potentiation-depression process at a finer timescale.

The underlying idea behind Eq. (3) is that each inhibitory neuron that is activated is likely to receive inputs from an overly excitatory region; in this way, by increasing its (inhibitory) weights it controls the excess of neighboring excitatory activity. Reciprocally, if an inhibitory neuron is inactive, weakening its weight promotes activity spreading and enhances local excitability.

To gauge excitatory-inhibitory balance in model simulations, we measure the mean input arriving at each single neuron and compute the corresponding probability distributions in the steady state [see Fig. 5(a)]. One can see that, in the absence of synaptic scaling (i.e., for the static case, shown in the left plot), heterogeneous networks (brown curve) exhibit an input distribution which is peaked at small positive values and has a large variance and a long tail, which reveals the existence of rare strong excitatory inputs. This is to be compared with the homogeneous case (blue curves) where the distribution of inputs is almost a δ function.

On the other hand, once synaptic scaling is switched on for heterogeneous networks, they self-organize to a steady-state input distribution which depends on the parameters η_p and η_d of the synaptic-plasticity rule [91] [see Fig. 5(a)], while it is rather insensitive to variations in ε. In particular, we distinguish two different regimes: a depression-dominated regime $\eta_p/\eta_d < 1$ and a potentiation-dominated regime for $\eta_p/\eta_d > 1$. In the depression-dominated regime, all inactive inhibitory neurons lose their weight quickly, thus leading to an excitatory-driven network in which there is a large average input with variability around it [central plots in Fig. 5(a)]. On the contrary, if potentiation dominates, the weight of inhibitory neurons increases significantly in the presence of activity, thus compensating quickly for excitatory inputs and driving the network towards a balanced state with close-to-zero inputs and much less dispersion than in the previous case [see the rightmost plots in Fig. 5(a)]. Therefore, the type of plasticity dominated by potentiation more closely resembles what is observed in actual biological networks.

Therefore, in the presence of a potentiation-dominated homeostatic mechanism the network self-organizes to a balanced asynchronous state, whereas the inputs almost vanish on average, giving rise to a fluctuation-dominated state with irregular activity [as evinced by, e.g., the large values of the CV in Fig. 5(b)], but without large dispersion in input values. Importantly, the degree of balance depends on the details of the adaptation mechanism; for instance, the CV is relatively small in the depression-dominated regime. Moreover, we observe that a progressively tighter balance can be achieved by further enhancing the ratio η_p/η_d with both parameters going to zero, a limit which resembles that of self-organized criticality [92].

Remarkably, Fig. 5(c) reports the steady-state distributions of inhibitory weights in the potentiation-dominated regime (for both homogeneous and heterogeneous networks). Such distributions exhibit a fat tail which spans for at least three decades and are larger for the heterogeneous case, in good agreement with previous theoretical and empirical observations that systematically report broad distributions of synaptic strengths [26,27,78].

IV. DISCUSSION

In this work, we have investigated the role of structural heterogeneity on the dynamics of spatially explicit excitation-inhibition networks. For this, we analyzed a parsimonious model of binary neurons [20,79]. Previous studies of such a model showed that the introduction of an inhibitory population on sparse random networks induces the emergence of an intermediate phase, in between the quiescent and saturated standard ones, of intermediate self-sustained activity, that does not exist in networks composed merely of excitatory neurons [20,83]. Such a phase exhibits all the properties of the asynchronous state [12–15,26]. However, previous studies did not carefully analyze the spatial structure or the possibility

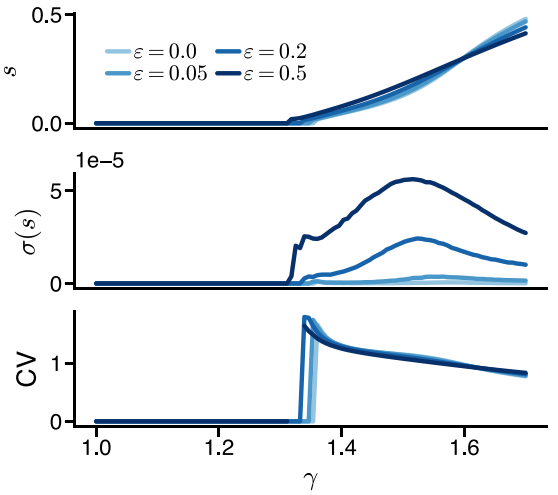

FIG. 6. Results for a different response function. From top to bottom, the average activity s, variance σ, and coefficient of variation are plotted as a function of γ for $f(x > 0) = \tanh(x)$. Note that the second transition becomes continuous, so the system does not saturate.

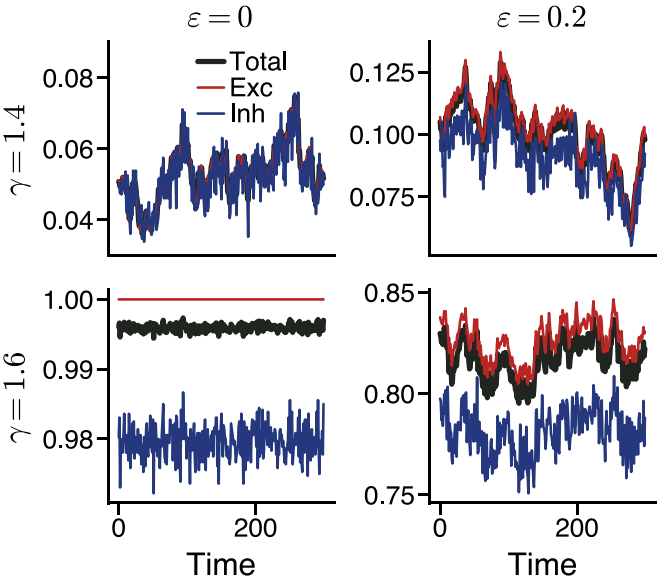

FIG. 7. Time series. The fraction of active neurons of the excitatory (red) and inhibitory (blue) populations and overall activity (black) are plotted as a function of time. Rows represent the time series for different coupling strengths, while columns are for different values of the heterogeneity parameter.

of structural heterogeneity and rare-region effects such as Griffiths phases (see, however, Ref. [29]).

When space is explicitly considered, as done here, there is neuronal clustering, i.e., nearby neurons tend to share a substantial proportion of neighbors, which is an essential feature of actual brain networks [23]. In particular, starting from a perfectly ordered and balanced network (the lattice shown in Fig. 1), we built heterogeneous spatially embedded networks by randomly relocating neurons in the embedding space in a progressive way. The breaking of homogeneity leads to the stochastic emergence of regions with an excess of excitatory neurons, where activity may reverberate for a long time, and regions where inhibition prevails, hindering activity propagation. As we have shown, this variability in local excitability produces smearing of the well-defined boundary between asynchronous and saturated phases, characteristic of homogeneous networks. Moreover, the resulting clustered structures lead to the emergence of a region in parameter space characterized by a generic scale-free slow relaxation, i.e., an identifying characteristic of a Griffiths phase. Such a variability of dynamical timescales could be crucial for enabling and shaping temporal input integration and segregation [93]. It is noteworthy that, in the absence of external input, activity may relax to the quiescent state before the synaptic-scaling mechanism has enough time to balance the network. In this sense, the slow dynamics of the Griffiths phase might have a role in allowing synaptic scaling (or other adaptation mechanisms) to fully develop (for a discussion on the network's response in finite time, see [94]).

In addition, we have also shown that structural heterogeneity promotes a more gradual recruitment of active neurons when an external input is applied, which significantly increases the overall dynamic range of the network, a highly desirable property in systems often exposed to sensory inputs that can range over several orders of magnitude. Such a network could also present advantages to store information locally and thus be efficient for working memory [95]. In general, the described dynamical regimes could potentially offer functional advantages for heterogeneous networks compared to homogeneous ones. However, our primary objective here was not to examine the potential functional benefits of each dynamical regime but rather to characterize them.

In order to reconcile heterogeneity with excitatory-inhibitory balance, we implemented (inspired by recent work by Landau *et al.* [78]) a synaptic-plasticity rule known as synaptic scaling [85,86], which requires only local information and that allows the network to adapt its behavior to diverse dynamical regimes. In particular, we have shown that synaptic scaling of inhibitory neurons suffices to dynamically restore the network balance in heterogeneous networks. Landau *et al.* found similar results for nonspatial networks of integrate-and-fire neurons [78]. Thus, our work extends the previous one by showing how synaptic scaling is able to restore the balance in spatially embedded networks. For these, heterogeneity induces stronger effects, including the emergence of rare regions and the concomitant Griffiths phases.

Finally, depending on the relative weight of synaptic potentiation and synaptic depression, networks can attain states closer to or farther from a typical asynchronous state in a self-organized manner. This makes it possible for such adaptive networks to achieve a variety of potential dynamical regimes, ranging from heterogeneous structures with unbalanced excitatory and inhibitory inputs to balanced asynchronous states, with different functional advantages for information processing. We leave for future work the study of this crossover between diverse dynamical regimes in biologically more realistic models, including, for example, the possibility of oscillations, i.e., a synchronization transition [96,97], and scrutiny of the potential functional advantages of adaptive networks exploiting this spectrum of possibilities, ranging from

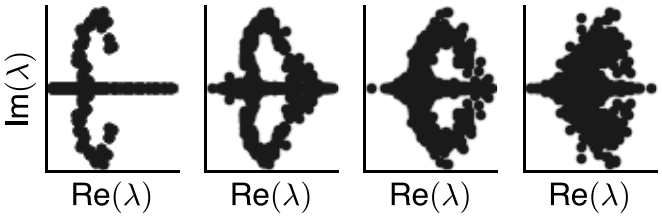

FIG. 8. Matrix spectra. Real and imaginary parts of the spectra of a matrix are generated using a system size with $L = 40$ (i.e., the matrix is 2000×2000) for increasing values of the heterogeneity parameter.

heterogeneity-dominated Griffiths-like states to asynchronous states. Finally, another long-term objective of ours is to contribute to the design of neuronal networks *in vitro* by achieving a suitable balance of excitation and inhibition [98,99].

ACKNOWLEDGMENTS

This research has been funded by the Spanish Ministry of Research and Innovation and Agencia Estatal de Investigación (AEI), MICIN/AEI/10.13039/501100011033 through Project Ref. PID2020-113681GB-I00. We also thank the Consejería de Conocimiento, Investigación Universidad, Junta de Andalucía and European Regional Development Fund (Grant No. P20-00173) for financial support. V.B. was supported by funding from the Sofja Kovalevskaja Award from the Alexander von Humboldt Foundation, endowed by the German Federal Ministry of Education and Research. We would like to thank A. Levina, R. Corral, G. B. Morales, R. Calvo, C. Martorell, S. di Santo, and Gustavo Menesse for insightful discussions and comments.

APPENDIX A: RESULTS FOR ANOTHER RESPONSE FUNCTION

We have confirmed that our main results remain unchanged when varying the considered response function, even if the nature of the second transition (irregular activity to saturation) can be affected by such a choice (we refer to the Supplemental Material of [20] for an in-depth discussion). In particular, Fig. 6 shows results analogous to those of Fig. 2 but using $f(x > 0) = \tanh(x)$ and $f(x \leqslant 0) = 0$. Observe that there is no significant change. Other properties, not reported here, also remain robust against changes in the response function.

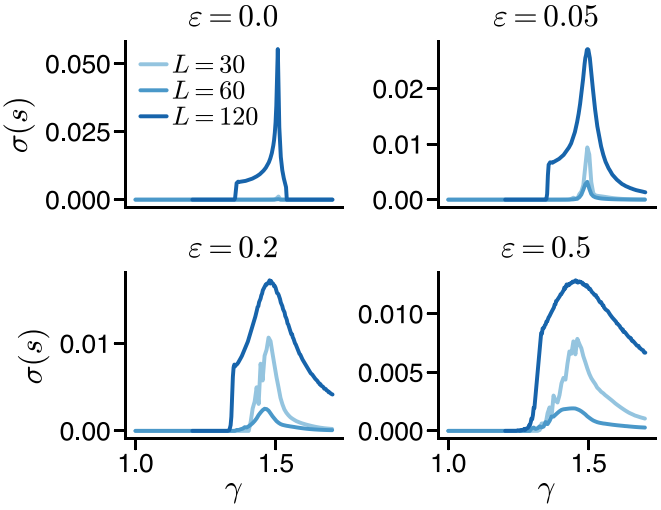

FIG. 9. Finite-size scaling. Variance of the activity is plotted as a function of the coupling strength γ for several system sizes. Note that $N = 5L^2/4$.

APPENDIX B: TIME SERIES

Figure 7 shows representative time series for two different couplings and two values of the heterogeneity parameter. Observe that in the homogeneous case (left column) $\gamma = 1.4$ lies within the asynchronous irregular regime, while $\gamma = 1.6$ is almost saturated. In the heterogeneous case (right column) there is no saturation and the irregular regime survives for larger values of γ.

APPENDIX C: NETWORK SPECTRA

For the sake of illustration, we report the spectra of the our adjacency matrices for different values of the heterogeneity parameter in Fig. 8. The behavior of the system is always dominated by the largest eigenvalue, but notice that for intermediate values of the heterogeneity there is a larger density of eigenvalues close to the leading one, leading to the slow timescales characteristic of the Griffiths phase [75].

APPENDIX D: FINITE-SIZE SCALING

We have performed a finite-size scaling of the phase diagram. We observe that variance of the activity tends to increase with the system size, as expected in critical phase transitions. Results are illustrated in Fig. 9.

[1] G. Deco, V. K. Jirsa, P. A. Robinson, M. Breakspear, and K. Friston, The dynamic brain: From spiking neurons to neural masses and cortical fields, PLoS Comput. Biol. **4**, e1000092 (2008).

[2] G. B. Morales, S. Di Santo, and M. A. Muñoz, Quasiuniversal scaling in mouse-brain neuronal activity stems from edge-of-instability critical dynamics, Proc. Natl. Acad. Sci. USA **120**, e2208998120 (2023).

[3] G. B. Morales, S. Di Santo, and M. A. Muñoz, Unveiling the intrinsic dynamics of biological and artificial neural networks: From criticality to optimal representations, arXiv:2307.10669

[4] G. Tononi, O. Sporns, and G. M. Edelman, A measure for brain complexity: Relating functional segregation and integration in the nervous system., Proc. Natl. Acad. Sci. USA **91**, 5033 (1994).

[5] G. Deco, G. Tononi, M. Boly, and M. L. Kringelbach, Rethinking segregation and integration: Contributions of whole-brain modelling, Nat. Rev. Neurosci. **16**, 430 (2015).

[6] O. Sporns, Network attributes for segregation and integration in the human brain, Curr. Opin. Neurobiol. **23**, 162 (2013).

[7] V. Buendía, P. Villegas, R. Burioni, and M. A. Muñoz, The broad edge of synchronization: Griffiths effects and collective

phenomena in brain networks, Philos. Trans. R. Soc. A **380**, 20200424 (2022).
[8] A. S. Ecker, P. Berens, G. A. Keliris, M. Bethge, N. K. Logothetis, and A. S. Tolias, Decorrelated neuronal firing in cortical microcircuits, Science **327**, 584 (2010).
[9] N. Dehghani, A. Peyrache, B. Telenczuk, M. Le Van Quyen, E. Halgren, S. S. Cash, N. G. Hatsopoulos, and A. Destexhe, Dynamic balance of excitation and inhibition in human and monkey neocortex, Sci. Rep. **6**, 1 (2016).
[10] C. Stringer, M. Pachitariu, N. Steinmetz, C. B. Reddy, M. Carandini, and K. D. Harris, Spontaneous behaviors drive multidimensional, brainwide activity, Science **364**, eaav7893 (2019).
[11] C. Stringer, M. Pachitariu, N. Steinmetz, M. Carandini, and K. D. Harris, High-dimensional geometry of population responses in visual cortex, Nature (London) **571**, 361 (2019).
[12] W. R. Softky and C. Koch, The highly irregular firing of cortical cells is inconsistent with temporal integration of random epsps, J. Neurosci. **13**, 334 (1993).
[13] A. Arieli, A. Sterkin, A. Grinvald, and A. Aertsen, Dynamics of ongoing activity: Explanation of the large variability in evoked cortical responses, Science **273**, 1868 (1996).
[14] M. Abeles, *Corticonics: Neural Circuits of the Cerebral Cortex* (Cambridge University Press, Cambridge, 1991).
[15] A. Renart, J. De La Rocha, P. Bartho, L. Hollender, N. Parga, A. Reyes, and K. D. Harris, The asynchronous state in cortical circuits, Science **327**, 587 (2010).
[16] C. van Vreeswijk and H. Sompolinsky, Chaos in neuronal networks with balanced excitatory and inhibitory activity, Science **274**, 1724 (1996).
[17] C. van Vreeswijk and H. Sompolinsky, Chaotic balanced state in a model of cortical circuits, Neural Comput. **10**, 1321 (1998).
[18] D. Hansel and H. Sompolinsky, Chaos and synchrony in a model of a hypercolumn in visual cortex, J. Comput. Neurosci. **3**, 7 (1996).
[19] R. Rubin, L. Abbott, and H. Sompolinsky, Balanced excitation and inhibition are required for high-capacity, noise-robust neuronal selectivity, Proc. Natl. Acad. Sci. USA **114**, E9366 (2017).
[20] V. Buendía, P. Villegas, S. Di Santo, A. Vezzani, R. Burioni, and M. A. Muñoz, Jensen's force and the statistical mechanics of cortical asynchronous states, Sci. Rep. **9**, 1 (2019).
[21] A. Alishbayli, J. G. Tichelaar, U. Gorska, M. X. Cohen, and B. Englitz, The asynchronous state's relation to large-scale potentials in cortex, J. Neurophysiol. **122**, 2206 (2019).
[22] N. Brunel, Dynamics of sparsely connected networks of excitatory and inhibitory spiking neurons, J. Comput. Neurosci. **8**, 183 (2000).
[23] E. Fino and R. Yuste, Dense inhibitory connectivity in neocortex, Neuron **69**, 1188 (2011).
[24] A. Fornito, A. Zalesky, and E. Bullmore, *Fundamentals of Brain Network Analysis* (Academic Press, New York, 2016).
[25] R. Rosenbaum, M. A. Smith, A. Kohn, J. E. Rubin, and B. Doiron, The spatial structure of correlated neuronal variability, Nat. Neurosci. **20**, 107 (2017).
[26] J.-n. Teramae, Y. Tsubo, and T. Fukai, Optimal spike-based communication in excitable networks with strong-sparse and weak-dense links, Sci. Rep. **2**, 485 (2012).
[27] G. Buzsáki and K. Mizuseki, The log-dynamic brain: How skewed distributions affect network operations, Nat. Rev. Neurosci. **15**, 264 (2014).
[28] A. Roxin, N. Brunel, D. Hansel, G. Mongillo, and C. van Vreeswijk, On the distribution of firing rates in networks of cortical neurons, J. Neurosci. **31**, 16217 (2011).
[29] D. Dahmen, M. Layer, L. Deutz, P. A. Dąbrowska, N. Voges, M. von Papen, T. Brochier, A. Riehle, M. Diesmann, S. Grün *et al.*, Global organization of neuronal activity only requires unstructured local connectivity, eLife **11**, e68422 (2022).
[30] V. Pernice, B. Staude, S. Cardanobile, and S. Rotter, How structure determines correlations in neuronal networks, PLoS Comput. Biol. **7**, e1002059 (2011).
[31] P. T. Sadtler, K. M. Quick, M. D. Golub, S. M. Chase, S. I. Ryu, E. C. Tyler-Kabara, B. M. Yu, and A. P. Batista, Neural constraints on learning, Nature (London) **512**, 423 (2014).
[32] J. A. Gallego, M. G. Perich, L. E. Miller, and S. A. Solla, Neural manifolds for the control of movement, Neuron **94**, 978 (2017).
[33] J. A. Gallego, M. G. Perich, S. N. Naufel, C. Ethier, S. A. Solla, and L. E. Miller, Cortical population activity within a preserved neural manifold underlies multiple motor behaviors, Nat. Commun. **9**, 4233 (2018).
[34] S. Denève and C. K. Machens, Efficient codes and balanced networks, Nat. Neurosci. **19**, 375 (2016).
[35] J. M. Beggs and D. Plenz, Neuronal avalanches in neocortical circuits, J. Neurosci. **23**, 11167 (2003).
[36] G. Hahn, T. Petermann, M. N. Havenith, S. Yu, W. Singer, D. Plenz, and D. Nikolić, Neuronal avalanches in spontaneous activity in vivo, J. Neurophysiol. **104**, 3312 (2010).
[37] A. J. Fontenele, J. S. Sooter, V. K. Norman, S. H. Gautam, and W. L. Shew, Low dimensional criticality embedded in high dimensional awake brain dynamics, bioRxiv:01.05.522896.
[38] E. Tagliazucchi, P. Balenzuela, D. Fraiman, and D. R. Chialvo, Criticality in large-scale brain fMRI dynamics unveiled by a novel point process analysis, Front. Physiol. **3**, 15 (2012).
[39] A. Ponce-Alvarez, A. Jouary, M. Privat, G. Deco, and G. Sumbre, Whole-brain neuronal activity displays crackling noise dynamics, Neuron **100**, 1446 (2018).
[40] A. Ponce-Alvarez, M. L. Kringelbach, and G. Deco, Critical scaling of whole-brain resting-state dynamics, Commun. Biol. **6**, 627 (2023).
[41] D. Plenz and E. Niebur, *Criticality in Neural Systems* (Wiley, New York, 2014).
[42] D. Plenz, T. L. Ribeiro, S. R. Miller, P. A. Kells, A. Vakili, and E. L. Capek, Self-organized criticality in the brain, Front. Phys. **9**, 639389 (2021).
[43] L. Cocchi, L. L. Gollo, A. Zalesky, and M. Breakspear, Criticality in the brain: A synthesis of neurobiology, models and cognition, Prog. Neurobiol. **158**, 132 (2017).
[44] M. A. Muñoz, *Colloquium*: Criticality and dynamical scaling in living systems, Rev. Mod. Phys. **90**, 031001 (2018).
[45] J. O'Byrne and K. Jerbi, How critical is brain criticality? Trends Neurosci. **45**, 820 (2022).
[46] M. Martinello, J. Hidalgo, A. Maritan, S. di Santo, D. Plenz, and M. A. Muñoz, Neutral theory and scale-free neural dynamics, Phys. Rev. X **7**, 041071 (2017).
[47] L. Meshulam, J. L. Gauthier, C. D. Brody, D. W. Tank, and W. Bialek, Coarse graining, fixed points, and scaling in a large population of neurons, Phys. Rev. Lett. **123**, 178103 (2019).
[48] S. A. Jones, J. H. Barfield, V. K. Norman, and W. L. Shew, Scale-free behavioral dynamics directly linked with scale-free cortical dynamics, eLife **12**, e79950 (2023).

[49] S. di Santo, P. Villegas, R. Burioni, and M. A. Muñoz, Simple unified view of branching process statistics: Random walks in balanced logarithmic potentials, Phys. Rev. E **95**, 032115 (2017).

[50] O. Sporns, D. R. Chialvo, M. Kaiser, and C. C. Hilgetag, Organization, development and function of complex brain networks, Trends Cognit. Sci. **8**, 418 (2004).

[51] J. M. Beggs, The criticality hypothesis: How local cortical networks might optimize information processing, Philos. Trans. R. Soc. A **366**, 329 (2008).

[52] J. Wilting and V. Priesemann, 25 years of criticality in neuroscience–established results, open controversies, novel concepts, Curr. Opin. Neurobiol. **58**, 105 (2019).

[53] W. L. Shew, H. Yang, S. Yu, R. Roy, and D. Plenz, Information capacity and transmission are maximized in balanced cortical networks with neuronal avalanches, J. Neurosci. **31**, 55 (2011).

[54] W. L. Shew and D. Plenz, The functional benefits of criticality in the cortex, Neuroscientist **19**, 88 (2013).

[55] A. Haimovici, E. Tagliazucchi, P. Balenzuela, and D. R. Chialvo, Brain organization into resting state networks emerges at criticality on a model of the human connectome, Phys. Rev. Lett. **110**, 178101 (2013).

[56] S. H. Gautam, T. T. Hoang, K. McClanahan, S. K. Grady, and W. L. Shew, Maximizing sensory dynamic range by tuning the cortical state to criticality, PLoS Comput. Biol. **11**, e1004576 (2015).

[57] W. L. Shew, W. P. Clawson, J. Pobst, Y. Karimipanah, N. C. Wright, and R. Wessel, Adaptation to sensory input tunes visual cortex to criticality, Nat. Phys. **11**, 659 (2015).

[58] D. Dahmen, S. Grün, M. Diesmann, and M. Helias, Second type of criticality in the brain uncovers rich multiple-neuron dynamics, Proc. Natl. Acad. Sci. USA **116**, 13051 (2019).

[59] J. Wilting and V. Priesemann, Between perfectly critical and fully irregular: A reverberating model captures and predicts cortical spike propagation, Cereb. Cortex **29**, 2759 (2019).

[60] J. Li and W. L. Shew, Tuning network dynamics from criticality to an asynchronous state, PLoS Comput. Biol. **16**, e1008268 (2020).

[61] O. Sporns, R. Kötter, and K. J. Friston, Motifs in brain networks, PLoS Biol. **2**, e369 (2004).

[62] O. Sporns, G. Tononi, and R. Kötter, The human connectome: A structural description of the human brain, PLoS Comput. Biol. **1**, e42 (2005).

[63] V. Balasubramanian, Heterogeneity and efficiency in the brain, Proc. IEEE **103**, 1346 (2015).

[64] J. F. Mejias and A. Longtin, Differential effects of excitatory and inhibitory heterogeneity on the gain and asynchronous state of sparse cortical networks, Front. Comput. Neurosci. **8**, 107 (2014).

[65] L. E. Suárez, R. D. Markello, R. F. Betzel, and B. Misic, Linking structure and function in macroscale brain networks, Trends Cognit. Sci. **24**, 302 (2020).

[66] L. Chen, C. Yu, and J. Zhai, How network structure affects the dynamics of a network of stochastic spiking neurons, Chaos **33**, 093101 (2023).

[67] J. Janarek, Z. Drogosz, J. Grela, J. K. Ochab, and P. Oświęcimka, Investigating structural and functional aspects of the brain's criticality in stroke, Sci. Rep. **13**, 12341 (2023).

[68] J. J. Binney, N. J. Dowrick, A. J. Fisher, and M. E. Newman, *The Theory of Critical Phenomena: An Introduction to the Renormalization Group* (Oxford University Press, Oxford, 1992).

[69] D. Sornette, *Critical Phenomena in Natural Sciences: Chaos, Fractals, Selforganization and Disorder: Concepts and Tools* (Springer Science+Business Media, New York, 2006).

[70] T. Vojta, Rare region effects at classical, quantum and nonequilibrium phase transitions, J. Phys. A: Math. Gen. **39**, R143 (2006).

[71] A. G. Moreira and R. Dickman, Critical dynamics of the contact process with quenched disorder, Phys. Rev. E **54**, R3090 (1996).

[72] R. Cafiero, A. Gabrielli, and M. A. Muñoz, Disordered one-dimensional contact process, Phys. Rev. E **57**, 5060 (1998).

[73] M. A. Muñoz, R. Juhász, C. Castellano, and G. Ódor, Griffiths phases on complex networks, Phys. Rev. Lett. **105**, 128701 (2010).

[74] R. Juhász, G. Ódor, C. Castellano, and M. A. Muñoz, Rare-region effects in the contact process on networks, Phys. Rev. E **85**, 066125 (2012).

[75] P. Moretti and M. A. Muñoz, Griffiths phases and the stretching of criticality in brain networks, Nat. Commun. **4**, 2521 (2013).

[76] G. Ódor, Robustness of Griffiths effects in homeostatic connectome models, Phys. Rev. E **99**, 012113 (2019).

[77] G. Ódor, Critical dynamics on a large human open connectome network, Phys. Rev. E **94**, 062411 (2016).

[78] I. D. Landau, R. Egger, V. J. Dercksen, M. Oberlaender, and H. Sompolinsky, The impact of structural heterogeneity on excitation-inhibition balance in cortical networks, Neuron **92**, 1106 (2016).

[79] D. B. Larremore, W. L. Shew, E. Ott, F. Sorrentino, and J. G. Restrepo, Inhibition causes ceaseless dynamics in networks of excitable nodes, Phys. Rev. Lett. **112**, 138103 (2014).

[80] M. Girardi-Schappo, L. Brochini, A. A. Costa, T. T. A. Carvalho, and O. Kinouchi, Synaptic balance due to homeostatically self-organized quasicritical dynamics, Phys. Rev. Res. **2**, 012042(R) (2020).

[81] R. P. Rocha, L. Koçillari, S. Suweis, M. Corbetta, and A. Maritan, Homeostatic plasticity and emergence of functional networks in a whole-brain model at criticality, Sci. Rep. **8**, 15682 (2018).

[82] G. Barzon, G. Nicoletti, B. Mariani, M. Formentin, and S. Suweis, Criticality and network structure drive emergent oscillations in a stochastic whole-brain model, J. Phys.: Complexity **3**, 025010 (2022).

[83] R. Corral López, V. Buendía, and M. A. Muñoz, Excitatory-inhibitory branching process: A parsimonious view of cortical asynchronous states, excitability, and criticality, Phys. Rev. Res. **4**, L042027 (2022).

[84] O. Kinouchi and M. Copelli, Optimal dynamical range of excitable networks at criticality, Nat. Phys. **2**, 348 (2006).

[85] Z. Ma, G. G. Turrigiano, R. Wessel, and K. B. Hengen, Cortical circuit dynamics are homeostatically tuned to criticality in vivo, Neuron **104**, 655 (2019).

[86] G. G. Turrigiano, The self-tuning neuron: Synaptic scaling of excitatory synapses, Cell **135**, 422 (2008).

[87] J. M. Cortes, D. Marinazzo, P. Series, M. W. Oram, T. J. Sejnowski, and M. C. Van Rossum, The effect of neural adaptation on population coding accuracy, J. Comput. Neurosci. **32**, 387 (2012).

[88] M. A. Gainey and D. E. Feldman, Multiple shared mechanisms for homeostatic plasticity in rodent somatosensory

and visual cortex, Philos. Trans. R. Soc. B **372**, 20160157 (2017).

[89] J. Zierenberg, J. Wilting, and V. Priesemann, Homeostatic plasticity and external input shape neural network dynamics, Phys. Rev. X **8**, 031018 (2018).

[90] G. Hennequin, E. J. Agnes, and T. P. Vogels, Inhibitory plasticity: Balance, control, and codependence, Annu. Rev. Neurosci. **40**, 557 (2017).

[91] V. Buendía, S. di Santo, P. Villegas, R. Burioni, and M. A. Muñoz, Self-organized bistability and its possible relevance for brain dynamics, Phys. Rev. Res. **2**, 013318 (2020).

[92] V. Buendía, S. Di Santo, J. A. Bonachela, and M. A. Muñoz, Feedback mechanisms for self-organization to the edge of a phase transition, Front. Phys. **8**, 333 (2020).

[93] A. Wolff, N. Berberian, M. Golesorkhi, J. Gomez-Pilar, F. Zilio, and G. Northoff, Intrinsic neural timescales: Temporal integration and segregation, Trends Cognit. Sci. **26**, 159 (2022).

[94] S. Azizpour, V. Priesemann, J. Zierenberg, and A. Levina, Available observation time regulates optimal balance between sensitivity and confidence, arXiv:2307.07794.

[95] J. F. Mejías and X.-J. Wang, Mechanisms of distributed working memory in a large-scale network of macaque neocortex, eLife **11**, e72136 (2022).

[96] S. di Santo, P. Villegas, R. Burioni, and M. A. Muñoz, Landau-Ginzburg theory of cortex dynamics: Scale-free avalanches emerge at the edge of synchronization, Proc. Natl. Acad. Sci. USA **115**, E1356 (2018).

[97] J. Liang, T. Zhou, and C. Zhou, Hopf bifurcation in mean field explains critical avalanches in excitation-inhibition balanced neuronal networks: A mechanism for multiscale variability, Front. Syst. Neurosci. **14**, 580011 (2020).

[98] H. Yamamoto, F. P. Spitzner, T. Takemuro, V. Buendía, H. Murota, C. Morante, T. Konno, S. Sato, A. Hirano-Iwata, A. Levina *et al.*, Modular architecture facilitates noise-driven control of synchrony in neuronal networks, Sci. Adv. **9**, eade1755 (2023).

[99] N. Sukenik, O. Vinogradov, E. Weinreb, M. Segal, A. Levina, and E. Moses, Neuronal circuits overcome imbalance in excitation and inhibition by adjusting connection numbers, Proc. Natl. Acad. Sci. USA **118**, e2018459118 (2021).